The mitochondrial respiratory chain is a modulator of apoptosis

Jennifer Q. Kwong, Matthew S. Henning, Anatoly A. Starkov, and Giovanni Manfredi

Department of Neurology and Neuroscience, Weill Medical College of Cornell University, New York, NY 10021

Mitochondrial dysfunction and dysregulation of apoptosis are implicated in many diseases such as cancer and neurodegeneration. We investigate here the role of respiratory chain (RC) dysfunction in apoptosis, using mitochondrial DNA mutations as genetic models. Although some mutations eliminate the entire RC, others target specific complexes, resulting in either decreased or complete loss of electron flux, which leads to impaired respiration and adenosine triphosphate (ATP) synthesis. Despite these similarities, significant differences in responses to apoptotic stimuli emerge. Cells lacking RC are protected against both mitochondrial- and endoplasmic reticulum (ER) stress–induced apoptosis. Cells with RC, but unable to generate electron flux, are protected against mitochondrial apoptosis, although they have increased sensitivity to ER stress. Finally, cells with a partial reduction in electron flux have increased apoptosis under both conditions. Our results show that the RC modulates apoptosis in a context-dependent manner independent of ATP production and that apoptotic responses are the result of the interplay between mitochondrial functional state and environmental cues.

Introduction

Mitochondria are responsible for aerobic respiration and ATP synthesis by oxidative phosphorylation. In addition to being crucial for energy production and metabolic pathways, they also play key roles in integrating cell death stimuli and executing the apoptotic program. Apoptosis plays an important role in development, morphogenesis, tissue remodeling, and diseases such as cancer and neurodegeneration. In the classical mitochondria-initiated apoptotic pathway, permeabilization of the mitochondrial outer membrane leads to cytochrome c release into the cytosol, formation of the apoptosome, and the subsequent activation of the caspase cascade (Spierings et al., 2005).

Another intracellular pathway of cell death involves ER stress. The ER is involved in the synthesis, folding, and modification of cell surface and secretory proteins, and is a key site for intracellular calcium storage. Disruption of these functions leads to the activation of the unfolded protein response.

Prolonged ER stress can lead to the accumulation of misfolded proteins, inhibition of protein glycosylation, and disruption of calcium homeostasis, which results in apoptosis (Xu et al., 2005). Although the mechanisms are still unclear, it is evident that ER stress engages the mitochondrial apoptotic pathways (Li et al., 2006).

Respiratory chain (RC) dysfunction is associated with mitochondrial diseases that affect tissues with high-energy demands such as brain, skeletal muscle, and heart (DiMauro and Schon, 2003). RC dysfunction has also been associated with neurodegenerative diseases such as Alzheimer's and Parkinson's disease (Kwong et al., 2006). The biogenesis of the mitochondrial RC is especially complex, as it is under the control of both the nuclear and mitochondrial genomes. The mitochondrial DNA (mtDNA) encodes for 13 polypeptides, all of which are integral subunits of the RC complexes (Anderson et al., 1981). Mutations in the mtDNA cause RC defects in some forms of mitochondrial disorders (DiMauro and Schon, 2003) but have also been shown to accumulate in normal aging (Kujoth et al., 2006) and in cancer (Polyak et al., 1998; Chatterjee et al., 2006). In the case of neurodegeneration and aging, it has been hypothesized that mtDNA mutations cause RC distress, which leads to mitochondrial dysfunction and apoptosis, whereas, in the case of cancer, RC dysfunction may confer resistance to apoptotic cell death. Therefore, dysregulation of apoptosis could be the link between RC defects and these divergent

Figure 1. **Characterization of the mtDNA mutant cell lines.** (A) Schematic representation of the human mtDNA. The mutants used in this study are indicated. (B) Coupled and uncoupled KCN-sensitive oxygen consumption was measured in whole cells with 1 mM pyruvate as a substrate. Cells were uncoupled with the addition of 1 μM FCCP. Cells harboring mtDNA mutations have severely reduced coupled and uncoupled respiration ($n = 6$; error bars represent SD).

pathophysiological extremes, but the mechanisms whereby the RC regulates apoptosis remain to be elucidated.

Here, we investigated the role of RC defects in regulating apoptotic cell death. We wanted to determine whether or not the effects of RC dysfunction on apoptosis varied depending on the loss of specific enzymatic activities. We used transmitochondrial cybrid cells harboring pathogenic mtDNA mutations as genetic tools to study targeted disruption of RC complexes. We compared the effects of a panel of diverse mtDNA mutations affecting different components of the RC on two different intracellular pathways of apoptosis. We focused on the mitochondria-initiated and the ER stress–induced pathways, because mitochondria and ER cooperate to form a functionally integrated system to maintain cellular homeostasis. We show that, although all the mtDNA mutations caused reduced mitochondrial respiration and ATP synthesis, they exhibited vastly different patterns of responses to mitochondrial and ER stress–mediated apoptotic stimuli. We identify the RC electron flux as a key modulator of apoptosis.

Results

MtDNA mutant cybrid cell lines

In this study, we used human osteosarcoma cybrid cells to examine different pathogenic mtDNA mutations against a common nuclear background. Cybrids were derived from the fusion of 143B ρ^0 cells, which are cells devoid of mtDNA, with enucleated cells from patients with mtDNA mutations (King and Attardi, 1989). All cybrid cell lines harbored homoplasmic levels of mutant mtDNA (i.e., 100% mutant).

The mutations we studied can be placed into three categories. The first consists of two mutations that affect single RC complexes, resulting in their disassembly and complete loss of function. It includes a stop-codon mutation at mtDNA nt 6930 in subunit I of complex IV (cytochrome c oxidase [COX]; Fig. 1 A), associated with mitochondrial encephalopathy (Bruno et al., 1999), and a 4–base pair microdeletion starting at position 14787 in the cytochrome b subunit of complex III (CYTB), associated with a form of parkinsonism and

Table I. **Characteristics of the mtDNA mutant cybrid cell lines used in this study**

Cell lines	RC complexes affected	MtDNA gene mutated	Nucleotide position of the mutation	Reference
ρ^0	I, III, IV, and V	No mtDNA	NA	King and Attardi, 1989
COX	IV	Cytochrome c oxidase subunit I	6390	Bruno et al., 1999
CYTB	III	Cytochrome b	Δ14787–14790	De Coo et al., 1999
MERRF	I, III, IV, and V	tRNA lysine	8344	Wallace et al., 1988
NARP	V	ATPase 6	8993	Holt et al., 1990

encephalopathy (De Coo et al., 1999). The second category includes a T–G transversion at position 8993 in the ATPase 6 gene (Holt et al., 1990), associated with neuropathy, ataxia, and retinitis pigmentosa (NARP). Unlike the other two protein-coding gene mutations, NARP affects complex V (F_1F_0 ATP synthase) function, but the protein complex itself is preserved (Cortes-Hernandez et al., 2007). The third category includes a point mutation at nt 8344 in the tRNA lysine gene (Wallace et al., 1988), which affects mtDNA protein synthesis resulting in a global loss of all RC complexes. This mutation is associated with a disease characterized by myoclonic epilepsy with ragged red fibers (MERRF). In addition, we studied parental 143B human osteosarcoma cells containing wild-type (WT) mtDNA and 143B ρ^0 cells (Table I).

Characterization of respiratory function in mtDNA mutants

To characterize the function of the RC in the various cybrid cell lines, we measured cyanide-sensitive oxygen consumption under both coupled (phosphorylating) and uncoupled (non-phosphorylating) states. As expected, ρ^0, COX, CYTB, and MERRF mutants had no respiration (Fig. 1 B), which is consistent with a complete blockage of RC electron transfer resulting from loss of RC complexes (D'Aurelio et al., 2006). NARP mutants had a partial impairment, with an ∼50% residual oxygen consumption as compared with WT. It was previously shown that the NARP mutation affects the ATPase complex and causes severely decreased ATP synthesis, resulting in a partial inhibition of RC activity (Fig. 1 B) and enhanced free radical production (Mattiazzi et al., 2004).

Mutant cybrids have different responses to apoptotic stimuli

Intrinsic apoptosis may be initiated through different cellular pathways that converge upon mitochondria. We set out to define the role that the RC and mtDNA mutations play in apoptosis, focusing on the mitochondria-initiated and the ER stress–induced pathways.

To engage the mitochondrial apoptotic pathway, we used staurosporine (STS) or etoposide (ET). As a quantitative measure of apoptosis, a caspase 3 fluorogenic assay was used. Treatment with STS resulted in reduced caspase 3 activation in ρ^0, COX, CYTB, and MERRF cybrids as compared with WT (Fig. 2 A). Interestingly, NARP cells had increased caspase 3 activation, suggesting that mtDNA mutations affecting the ATPase complex behave differently than those affecting the RC. The pattern of apoptotic response to STS was confirmed by staining for

apoptotic nuclei (Fig. S1 A, available at http://www.jcb.org/cgi/content/full/jcb.200704059/DC1). ET showed a pattern of apoptosis very similar to STS, although the trend for reduced response did not reach statistical significance in the COX cybrids (Fig. 2 B). As expected, ET treatment resulted in cleavage of caspases 9 and 3, as detected by Western blot, supporting the findings of the fluorogenic assays (Fig. S2 A).

Treatment with thapsigargin (TG) to activate the ER stress pathways of apoptosis by inhibiting the sarcoplasmic reticulum/ER Ca^{2+} ATPase showed a remarkably different pattern of caspase 3 activation. Although ρ^0 and MERRF cells were protected, COX, CYTB, and NARP had increased caspase 3 activation (Fig. 2 C). These results were confirmed by annexin V and propidium iodide staining (Fig. S1 B). TG treatment also resulted in cleavage of caspases 9 and 3 (Fig. S2 B). A pattern of response similar to that of TG was observed using tunicamycin (TN), which induces the ER stress response through a different mechanism by inhibiting protein glycosylation (Fig. 2 D).

To confirm that the pathways leading to cell death in our cybrid cells were indeed dependent on caspase activation, we measured cell survival after treatment with proapoptotic compounds, with or without the addition of the pan-caspase inhibitor ZVAD-fluoromethylketone in one of the mutant cell lines. As expected, STS, TG, and ET reduced cell viability, as determined by the WST-1 live cell assay, and ZVAD-fluoromethylketone completely prevented cell death (Fig. S2 C).

To discount the possibility that the effects we saw in response to TG could be specific to individual cybrid clones, we confirmed the results in rederived new MERRF cybrid mass cultures, obtained by fusion of enucleated MERRF cells with osteosarcoma ρ^0 cells, and in two additional NARP clones (Fig. S3, available at http://www.jcb.org/cgi/content/full/jcb.200704059/DC1). Furthermore, to exclude the idea that the protection against TG in ρ^0 and MERRF mutants was specific to osteosarcoma cells, we confirmed the results in ρ^0 (Fig. S3 B) and MERRF mutants (not depicted) generated in a HeLa nuclear background.

Collectively, these results indicate that the various categories of mtDNA mutations display clear differences in their responses to proapoptotic stimuli and that even within the same category of mutation, the apoptotic response varies depending on the type of stimulus.

Correlation between the mitochondrial energetic state and STS-induced apoptosis

We noted that cybrid cell lines harboring mtDNA mutations that disrupted mitochondrial respiration were protected against STS-induced apoptosis. Therefore, we hypothesized that the
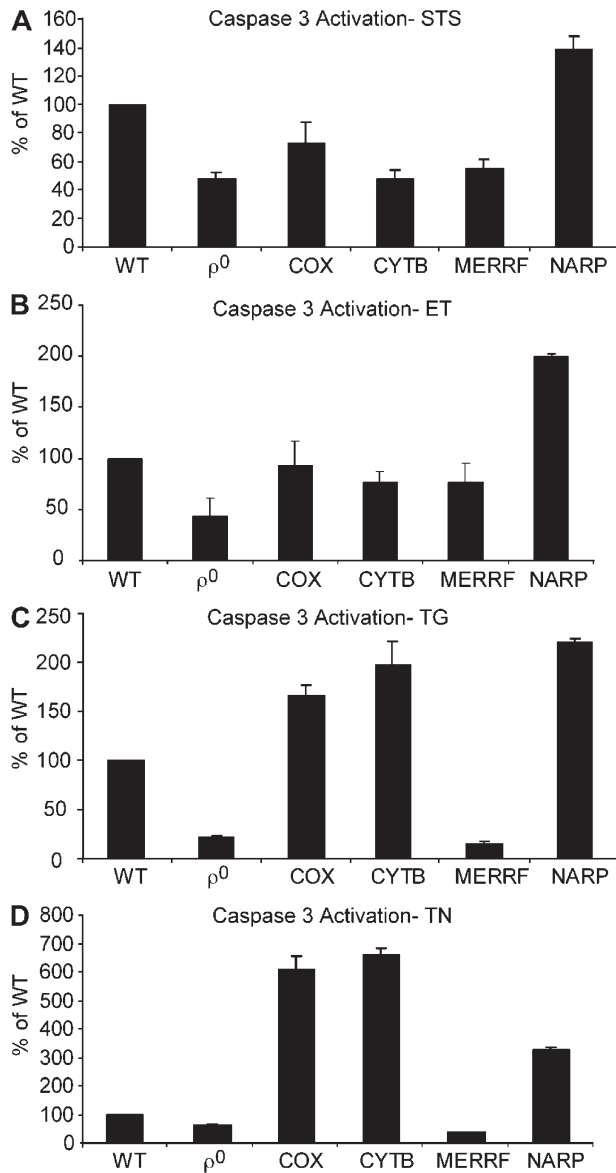
Figure 2. **Apoptosis in the mtDNA mutant cybrid cells.** (A) Caspase 3 activity in response to 1 μM STS for 6 h, expressed as a percentage of the response observed in WT cells ($n = 4$; error bars represent SEM). ρ^0, COX, CYTB, and MERRF cells are protected, whereas NARP cells are hypersensitive to STS-induced caspase 3 activation. (B) Caspase 3 activity in response to 10 μM ET for 24 h, expressed as a percentage of the response observed in WT cells ($n = 4$; error bars represent SEM). ρ^0, MERRF, COX, and CYTB show a trend for protection, whereas NARP cells are hypersensitive to ET-induced caspase 3 activation. (C) Caspase 3 activity in response to 1 μM TG for 24 h, expressed as a percentage of the response observed in WT cells ($n = 8$; error bars represent SEM). ρ^0 and MERRF cells were protected against TG, whereas COX, CYTB, and NARP cells were hypersensitive to TG. (D) Caspase 3 activity in response to 1 μM TN for 24 h, expressed as a percentage of the response observed in WT cells ($n = 4$; error bars represent SEM). The pattern of TN-induced caspase 3 activity mirrored the pattern induced by TG (C).

mitochondrial energetic state may be a key regulator of this apoptotic pathway. To examine this hypothesis, we studied the ability of mutant mitochondria to generate membrane potential ($\Delta\Psi_m$) using their RC. As expected, NARP mitochondria, which possess all of the RC complexes, generated $\Delta\Psi_m$ (Fig. 3 A),

albeit at a lower capacity than WT, which is consistent with a reduction in respiration (Fig. 1 B). All of the other mutants were unable to generate $\Delta\Psi_m$, which is consistent with a complete block in electron transport (Fig. 1 B).

Cells with fragmented mitochondria are protected against STS-induced apoptosis

It has been shown that loss of $\Delta\Psi_m$ results in a fragmentation of the mitochondrial network (Legros et al., 2002) and that ρ^0 cells have altered mitochondrial morphology (Gilkerson et al., 2000). In our mutant cybrids, confocal microscopy of cells stained with the mitochondria-specific dye MitoTracker Red revealed a normal tubular network in WT and NARP cells, whereas ρ^0, COX, CYTB, and MERRF cells had fragmented mitochondria (Fig. 3 C). Measurement of mitochondrial length showed that these mutants have shorter mitochondria (Fig. 3 D). By arbitrarily categorizing mitochondria based on size, WT and NARP cells have an approximately equal distribution of long (>2 μm) and short (<2 μm) mitochondria, whereas ρ^0, COX, CYTB, and MERRF cells have almost exclusively short mitochondria (Fig. 3 E). These results indicate a strong correlation between the loss of electron transfer and the disruption of the mitochondrial network. They also suggest that morphological changes are correlated with the pattern of sensitivity to mitochondrial stressors but not that of ER stressors, as all cells with fragmented mitochondria were protected against STS or ET-induced apoptosis but COX and CYTB cells were highly sensitive to TG and TN.

MtDNA mutations do not affect the induction of the ER stress–response pathway

The response to ER stress–induced cell death did not follow the same pattern as that of mitochondrial-induced cell death because some of the mutants that displayed the highest caspase activation (Fig. 2, C and D, COX and CYTB) were protected against STS- and ET-induced death (Fig. 2, A and B). To determine if the differences observed in TG-induced apoptosis were caused by differential ER stress responses, we monitored the levels of the ER stress marker Grp78 (Li et al., 2006). We found that all cell lines up-regulated Grp78 equally after TG treatment (Fig. 4). Therefore, we concluded that mtDNA mutations do not affect the cell's ability to mount an ER stress response and that this pathway was intact and activated in all cell lines.

Mitochondrial ATP synthesis is not required for ER stress–induced apoptosis and ER stress does not result in acute ATP depletion

Because apoptosis and caspase activation are energy-dependent processes, we tested whether defective mitochondrial ATP production plays a role in modulating ER stress– induced apoptosis. To completely inhibit mitochondrial ATP synthesis, WT cells were treated with the ATP synthase inhibitor oligomycin in combination with TG. Oligomycin had no significant effect on TG-induced caspase 3 activation as compared with TG treatment alone (Fig. 5 A). However, it caused increased caspase 3 activation in ρ^0, COX, CYTB, and MERRF cells. Collectively,
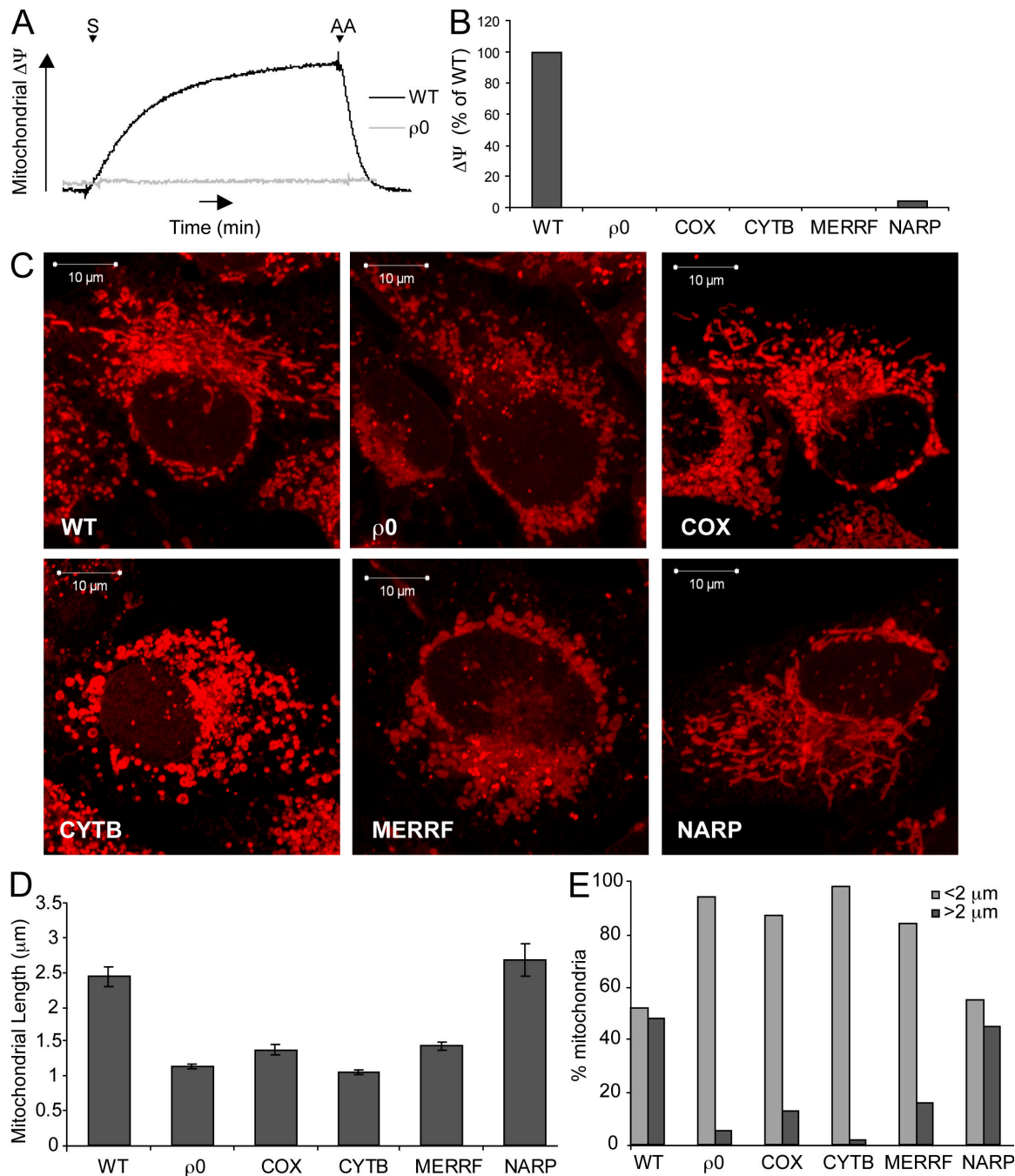
Figure 3. **ΔΨ$_m$ generated by the RC is necessary to maintain normal mitochondrial morphology.** (A) Representative traces of the ΔΨ$_m$ generated in isolated mitochondria from WT and ρ^0 cells. Incubation medium (see Materials and methods) was supplemented with 5 mM succinate (S). 1 μM antimycin A was added to deenergize mitochondria (AA). (B) Quantification of ΔΨ$_m$ generated in mtDNA mutant cells ($n = 3$). Only WT and NARP cells were able to generate RC-supported ΔΨ$_m$. (C) Confocal images of cells stained with 100 nM MitoTracker Red CMXRos for 30 min at 37°C. WT and NARP cells have intact mitochondrial networks, whereas ρ^0, COX, CYTB, and MERRF cells display fragmented and punctate mitochondrial morphology. (D) Mean mitochondrial length in the mtDNA mutant cybrids. ρ^0, COX, CYTB, and MERRF mitochondria had significantly decreased mean lengths as compared with WT and NARP mitochondria. 100 mitochondria were scored for each cell line (error bars represent SEM). (E) Distribution of mitochondrial lengths in the various cell lines. ρ^0, COX, CYTB, and MERRF cells had a significant decrease in the proportion of mitochondria >2 μm.

these results indicate that mitochondrial ATP synthesis is not necessary for TG-induced caspase activation and that glycolytic ATP is sufficient to drive ER stress–induced apoptosis. However, because oligomycin inhibits both mitochondrial ATP synthesis and hydrolysis and cells lacking RC function may be actively consuming ATP in mitochondria, these results also

suggest that oligomycin may actually increase the pool of ATP available for caspase activation in mutant cells.

It has been shown that a transient decrease in cellular ATP levels can commit cells to apoptosis (Izyumov et al., 2004). To determine the effect of ER stress on cellular steady-state ATP levels, ATP content was monitored during TG treatment at time
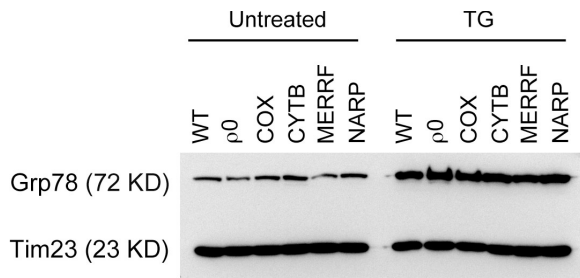
Figure 4. **ER stress is induced equally in mtDNA mutant cells.** Western blot of the ER stress marker Grp78. TG treatment (1 μM for 24 h) strongly up-regulated Grp78 protein expression in all cell lines. Tim23, a protein unaffected by ER stress, was used as a loading control.

points preceding any appreciable cell death. Over a 3-h period, there was no change in ATP content in any of the cell lines tested (Fig. 5 B). Therefore, we concluded that acute ATP depletion does not play a role in this mode of cell death and cannot explain the different responses in the various mutant cell lines.

Acute mitochondrial uptake of ER Ca²⁺ released by TG in mutant cybrids

Both the mitochondria and ER cooperate in maintaining intracellular Ca^{2+} homeostasis. Acute mitochondrial uptake of Ca^{2+} released upon ER stress may trigger mitochondrial permeability transition and the release of proapototic factors. To test this possibility, we treated cells with TG and the permeability transition pore inhibitor cyclosporine A. Cyclosporine A did not protect

against TG-induced caspase 3 activation in any of the cell lines (unpublished data). Therefore, we concluded that in our model, Ca^{2+}-mediated permeability transition does not play a role in ER stress–induced apoptosis.

To further investigate whether differential Ca^{2+} uptake may play a role in TG sensitivity, we compared the amount of Ca^{2+} taken up into mitochondria after TG stimulation in the various cell lines. Changes in cytosolic Ca^{2+} in intact cells were monitored using Fura 2AM. First, cytosolic Ca^{2+} was measured before and after the addition of FCCP to release mitochondrial Ca^{2+} (Fig. 6 A). The difference in cytosolic Ca^{2+} before and after carbonylcyanide-*p*-trifluoromethoxyphenylhydrazone (FCCP) was taken as a measure of basal mitochondrial Ca^{2+} stores (Fig. 6 A, mCa before). Ca^{2+} was then released from the ER using TG, followed by release of Ca^{2+} from the mitochondria using FCCP (Fig. 6 B, mCa after). The difference in cytosolic Ca^{2+} levels between the two FCCP-induced Ca^{2+} peaks (Fig. 6 C) was indicative of the amount of Ca^{2+} taken up into the mitochondria after TG stimulation. If acute mitochondrial Ca^{2+} uptake was the signal that triggers the apoptotic response, then one would expect that mitochondria from cell lines with normal or increased TG sensitivity should be able to take up Ca^{2+}, whereas mitochondria from cells with reduced sensitivity should not. Consistent with this hypothesis, we found that ρ^0 and MERRF cells, which are protected against TG-induced death, did not take up additional Ca^{2+} after TG, whereas COX and CYTB cells, which are more sensitive to TG, did (Fig. 6 C). However, NARP cells, which also have increased sensitivity to TG, were unable to take up Ca^{2+}.
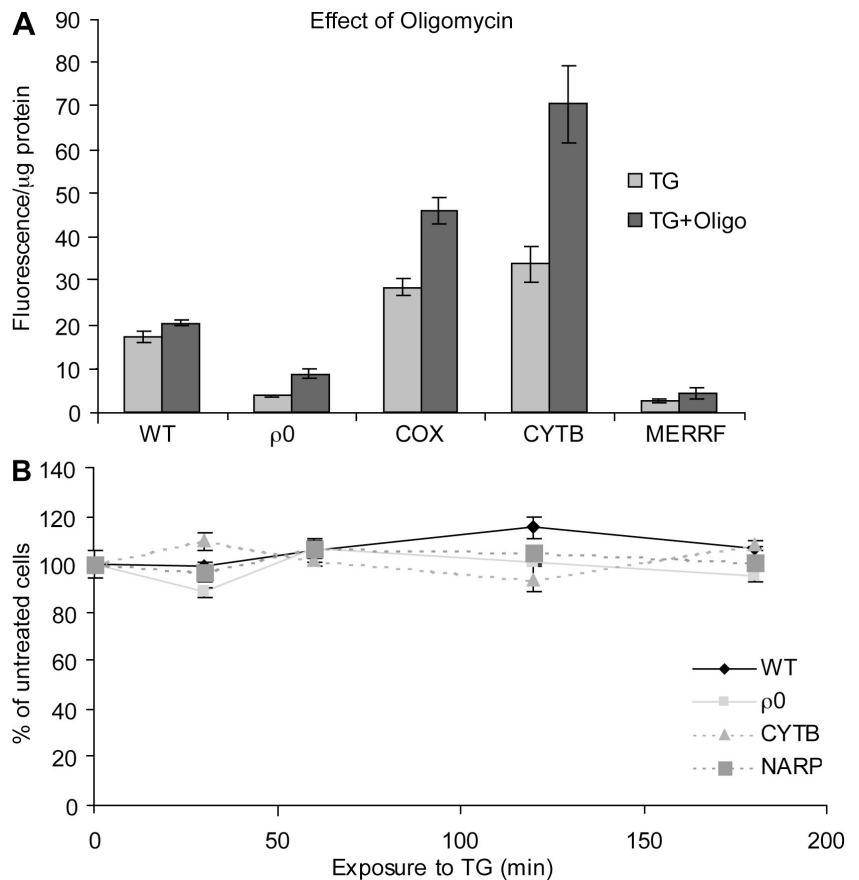

Figure 5. **Mitochondrial ATP synthesis and cellular ATP content are not implicated in ER stress–induced apoptosis.** (A) Caspase 3 activity in cells treated with either 1 μM TG alone or 1 μg/ml TG in combination with the mitochondrial ATP synthase inhibitor oligomycin for 24 h (n = 6; error bars represent SEM). Inhibition of ATP synthase did not modify the response in WT cells, whereas mutant cells exhibited increased caspase activity. (B) WT, ρ^0, CYTB, and NARP cells were treated with 1 μM TG for various times and total cellular ATP content was measured (n = 3; error bars represent SEM). ATP content at each time point is expressed as a percentage of the untreated values, suggesting that acute ER stress does not result in ATP depletion.

This unexpected result was replicated in another, independent NARP cell line derived from a different patient (unpublished data), suggesting that in these mutants other factors may contribute to enhanced sensitivity to ER stress.

Mitochondrial uptake of Ca^{2+} depends on $\Delta\Psi_m$, which can be generated either by using the RC or by the reverse action of the ATPase complex that hydrolyzes ATP to pump protons from the matrix into the intermembrane space. To determine if the differences in mitochondrial uptake of Ca^{2+} released from the ER correlated with bioenergetics, we examined the ability of isolated mitochondria to take up Ca^{2+} in the presence of different substrates and increasing Ca^{2+} concentrations. With RC substrates, WT mitochondria and to a much lower extent NARP mitochondria were able to take up Ca^{2+}, whereas ρ^0, COX, CYTB, and MERRF mitochondria were not, as shown in the representative traces from WT and ρ^0 mitochondria (Fig. 7, A and B). However, when the mitochondria were forced to hydrolyze ATP to generate $\Delta\Psi_m$, WT, COX, and CYTB mitochondria were able to take up Ca^{2+}, whereas ρ^0, MERRF, and NARP mitochondria were not (unpublished data). In summary, WT mitochondria can use both RC- and ATP hydrolysis–driven $\Delta\Psi_m$ for acute Ca^{2+} uptake, ρ^0 and MERRF mitochondria cannot take up Ca^{2+} by either mechanism, NARP mitochondria display a limited ability to take up Ca^{2+} using the RC, and COX and CYTB mitochondria can take up Ca^{2+} but only by expending ATP.

As described in the previous paragraph, only WT and NARP cells were able to use RC substrates to generate $\Delta\Psi_m$ (Fig. 3 A). To further study how the modality of $\Delta\Psi_m$ generation correlates with the Ca^{2+} uptake, we measured the ability of isolated mitochondria to generate $\Delta\Psi_m$ using ATP as a substrate. WT, COX, CYTB, and to a smaller extent NARP and MERRF cells were able to generate $\Delta\Psi_m$ under these conditions (Fig. 7, C and D).

Collectively, these observations show that there is a correlation between generation of $\Delta\Psi_m$ and the ability to take up Ca^{2+} by mitochondria. This correlation is reflected in the sensitivity to TG-induced apoptosis, with the exception of NARP cells. Cells that generate no or low $\Delta\Psi_m$ (ρ^0 and MERRF) have no Ca^{2+} uptake and are protected against apoptosis. Cells that are able to generate $\Delta\Psi_m$ (WT, COX, and CYTB) do uptake Ca^{2+} and can
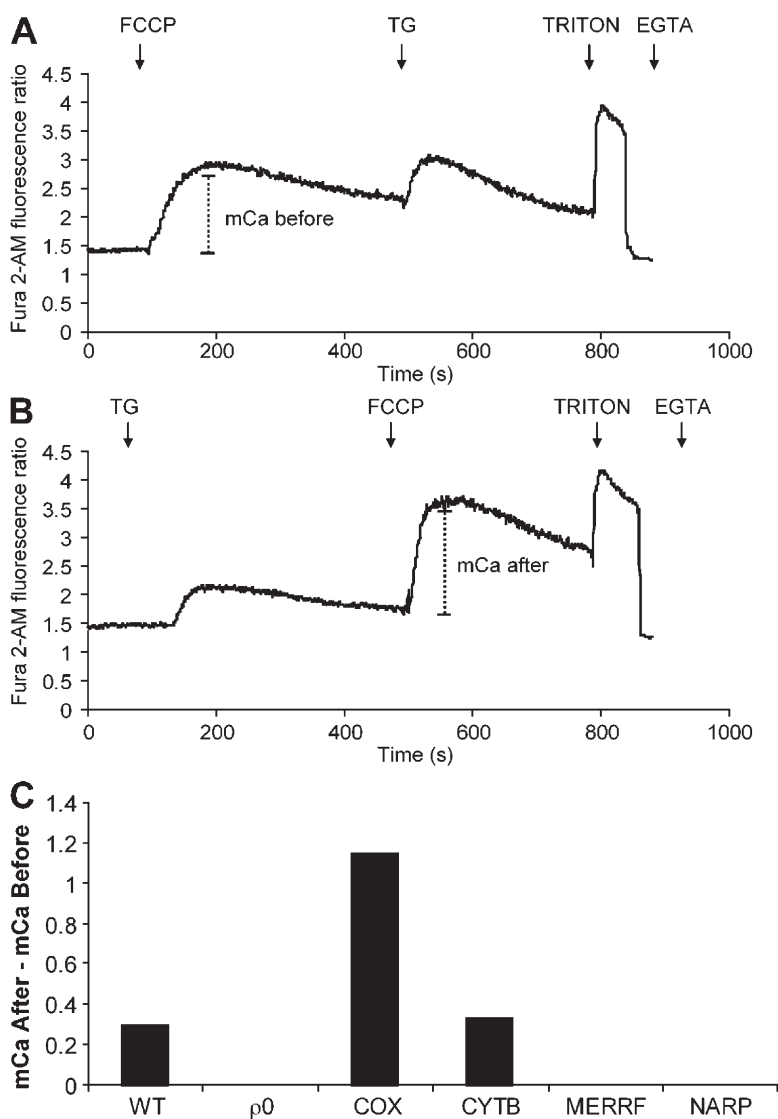

Figure 6. **Acute mitochondrial Ca^{2+} uptake upon ER stress does not correlate with the pattern of ER stress–induced apoptosis.** (A and B) Representative traces of fluorometric measurement of cytosolic Ca^{2+} levels are shown using the Ca^{2+}-sensitive dye Fura 2AM. Mitochondrial Ca^{2+} stores were released with FCCP and ER calcium stores were released by the addition of TG. The amount of Ca^{2+} in mitochondria was measured before (A, mCa before) and after ER calcium release with TG (B, mCa after). (C) Quantification of mitochondrial Ca^{2+} uptake after TG treatment. The amount of Ca^{2+} taken up by mitochondria in the mtDNA mutant cell lines after Ca^{2+} release by the ER was quantified by measuring the difference between mCa after and mCa before.
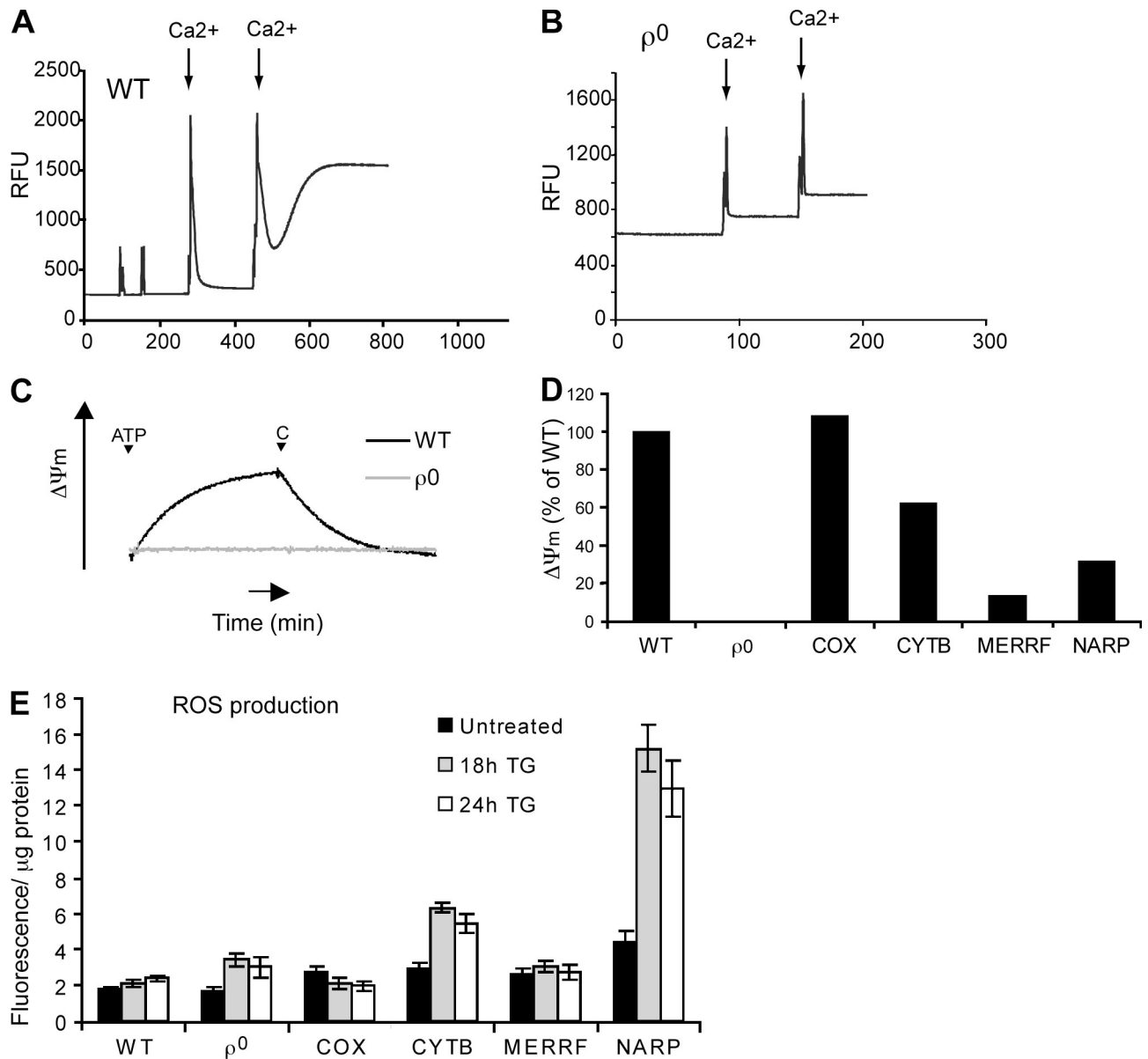
Figure 7. **Mitochondrial Ca²⁺ uptake correlates with the ability to maintain ΔΨₘ.** (A) Representative trace of Ca²⁺ uptake in isolated WT mitochondria. 100 µg mitochondria were incubated in buffer containing Calcium Green-5N, 7 mM pyruvate, and 1 mM of the RC substrate malate. Mitochondria were challenged with sequential additions of 100 nmol CaCl₂ (arrows). After each addition there is a spike in fluorescence caused by increase Ca²⁺ concentration in the buffer. The downward slope reflects mitochondrial uptake of Ca²⁺. Note that under these conditions, WT mitochondria undergo permeability transition as indicated by release of Ca²⁺ in the buffer. (B) Representative trace of lack of Ca²⁺ uptake in isolated mitochondria from ρ⁰ cells. In comparison to A, it is clear that there is no progressive mitochondrial Ca²⁺ uptake, but the fluorescence increases stepwise because of increased concentration of Ca²⁺ in the buffer. (C) Representative traces of the ATP-supported ΔΨₘ generation in WT and ρ⁰ mitochondria. ΔΨₘ supported by ATP hydrolysis was taken as the difference between the maximal signal generated with the addition of ATP and the minimal signal generated with the addition of carboxyatractylate (C). (D) Quantification of ΔΨₘ generated by ATP hydrolysis in cybrid cell lines ($n = 3$). WT, COX, CYTB, MERRF, and NARP mitochondria were able to generate ΔΨₘ using ATP as a substrate, whereas ρ⁰ mitochondria were not. (E) ROS production before and after stimulation with 1 µM TG. Hydroperoxides measured with H₂DCFDA are expressed as fluorescence units per micrograms of cellular proteins. NARP and CYTB cells have significantly increased ROS at 18 and 24 h after TG. Error bars represent SEM.

mount a normal or high apoptotic response. However, the NARP cybrids represent an exception because they are only able to generate a modest ΔΨₘ (Figs. 3 A and 7 D) and uptake very low Ca²⁺ in isolated mitochondria and none in whole cells (Fig. 6 C), and yet they are highly sensitive to TG (Fig. 2 C). Therefore, the results in NARP cells support the conclusion that in these cells the sensitivity to ER stress–induced apoptosis cannot be ascribed exclusively to acute mitochondrial Ca²⁺ uptake.

Free radical production is increased in NARP cells in response to ER stress

We have previously demonstrated that NARP cells have increased production of reactive oxygen species (ROS) under normal growth conditions (Mattiazzi et al., 2004). Increased ROS have also been associated with enhanced apoptosis in NARP fibroblasts, which could be prevented by antioxidants (Geromel et al., 2001). We measured ROS production in cybrids before
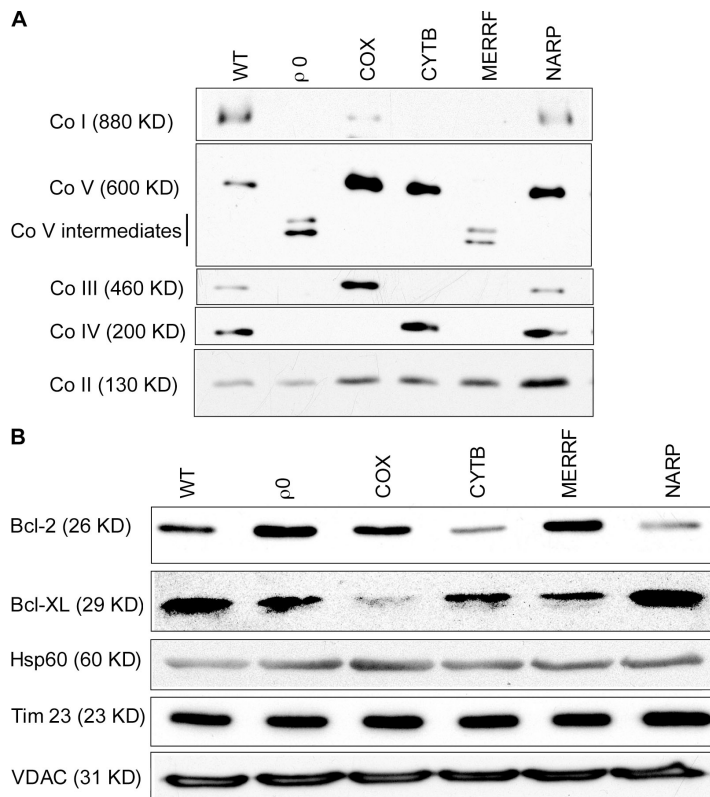
Figure 8. **BN gels of RC complexes and mitochondrial levels of anti-apoptotic Bcl-2 proteins.** (A) WT cells have a full complement of RC complexes, whereas ρ^0 and MERRF cells lack assembled complexes containing mtDNA-specified subunits (complexes I, III, IV, and V) and have partially assembled complex V intermediates. COX cells lack complex IV and have reduced complex I. CYTB cells lack complex III and also have severely reduced complex I. NARP cells contain all five RC complexes. (B) Western blot of the antiapoptotic proteins Bcl-2 and Bcl-X$_L$ in enriched mitochondrial fractions. Hsp60 was used as a marker of the mitochondrial matrix, Tim23 was used as a marker of the mitochondrial inner membrane, and VDAC was used as a marker of the mitochondrial outer membrane.

and after treatment with STS or TG and confirmed that baseline ROS production was increased in NARP cells. However, after STS treatment, no significant increase in ROS was observed in any of the cell lines (unpublished data), whereas TG induced a dramatic fourfold increase in ROS production in NARP cybrids (Fig. 7 E). Among the other cybrid lines, only CYTB showed a significant ROS elevation in response to TG, but to a much lesser extent than NARP. These results suggest that ROS production could be a major contributor to the increased sensitivity of NARP cells to ER stress–induced apoptosis.

The mitochondrial RC is required to mount a normal apoptotic response to ER stress

Despite the fact that all of our mtDNA mutant lines have an impaired RC, our data clearly indicate that there are differences among the mutants in the way mitochondria attempt to maintain $\Delta\Psi_m$ and in Ca^{2+} handling. Therefore, we hypothesized that such differences could be the result of changes in RC composition. Blue native (BN) gel electrophoresis followed by immunoblotting with RC-specific antibodies was used to study RC assembly. As expected, ρ^0 cells, which lack mtDNA, did not have assembled complexes I, III, IV, and V, as all of these complexes include mtDNA-specified subunits (Fig. 8 A). ρ^0 cells only retained assembled complex II, which is entirely encoded by the nuclear genome. MERRF cells, which have a severe mitochondrial protein synthesis defect, also lacked detectable amounts of mtDNA-encoded complexes. Note that MERRF cells must have a small proportion of residual RC, below the level of detection by BN-Western blot, because they are capable of low-level oxygen consumption (Fig. 1 B) and ATP hydrolysis (Fig. 7 D).

In COX cells, complex IV was absent and complex I was reduced, as previously reported (D'Aurelio et al., 2006), but complexes II, III, and V were present (Fig. 8 A). CYTB cells revealed a complete loss of complex III and a concomitant severe reduction in complex I (Acin-Perez et al., 2004), but had fully assembled complexes II, IV, and V. Finally, NARP cells had all of the respiratory components assembled.

The pattern of RC assembly correlates with mitochondrial bioenergetics. Because COX and CYTB mutants lack critical complexes for electron flux but retain complex V, their mitochondria can only generate $\Delta\Psi_m$ by ATP hydrolysis. ρ^0 and MERRF cells lack the RC and electron flux and therefore are unable to generate $\Delta\Psi_m$ either by respiration or ATP hydrolysis. NARP cells, which have a functional impairment of ATPase resulting in an upstream reduction of electron flux and increased ROS production (Mattiazzi et al., 2004), have an impairment in both mechanisms despite having an assembled RC.

Collectively, our data suggest that the presence of an assembled RC is required to mount a normal apoptotic response. However, when some RC components are present but the electron flux is disrupted, cells have increased sensitivity to ER stress–induced apoptosis.

The RC regulates levels of antiapoptotic proteins at the mitochondria

It is well established that the Bcl-2 family of proteins is important in modulating apoptosis (Danial and Korsmeyer, 2004). It has previously been reported that cells with mtDNA depletion have increased expression of the antiapoptotic protein Bcl-2 (Biswas et al., 2005b). We confirmed this finding in enriched

Figure 9. **Electron flux through mitochondrial RC modulates ER stress–induced apoptosis.** (A) Caspase 3 activation in response to TG and FCCP. Cells were pretreated with 5 μM FCCP for 30 min and then cotreated with 1 μM TG for 24 h. The effect of FCCP on TG-induced caspase 3 activation is expressed as a percentage of protection as compared with the TG treatment alone ($n = 4$; error bars represent SEM). (B) Caspase 3 activation in response to TG and TMPD. Cells were pretreated with 140 μM TMPD for 30 min and then cotreated with 1 μM TG for 24 h. Caspase 3 activity in WT cells treated with both TG and TMPD is defined as 100% ($n = 4$; error bars represent SEM). (C) Caspase 3 activity in untreated or 1-μM TG-treated WT cells with or without the addition of 100 nM of RC inhibitor rotenone, 4 μM of RC inhibitor piericidin A, and 1 μM of RC inhibitor antimycin A for 24 h. Caspase 3 activity is expressed as a percentage of WT cells treated with TG alone (set at 100%; $n = 3$; error bars represent SEM). All inhibitors of the RC enhance the apoptotic response in WT cells.
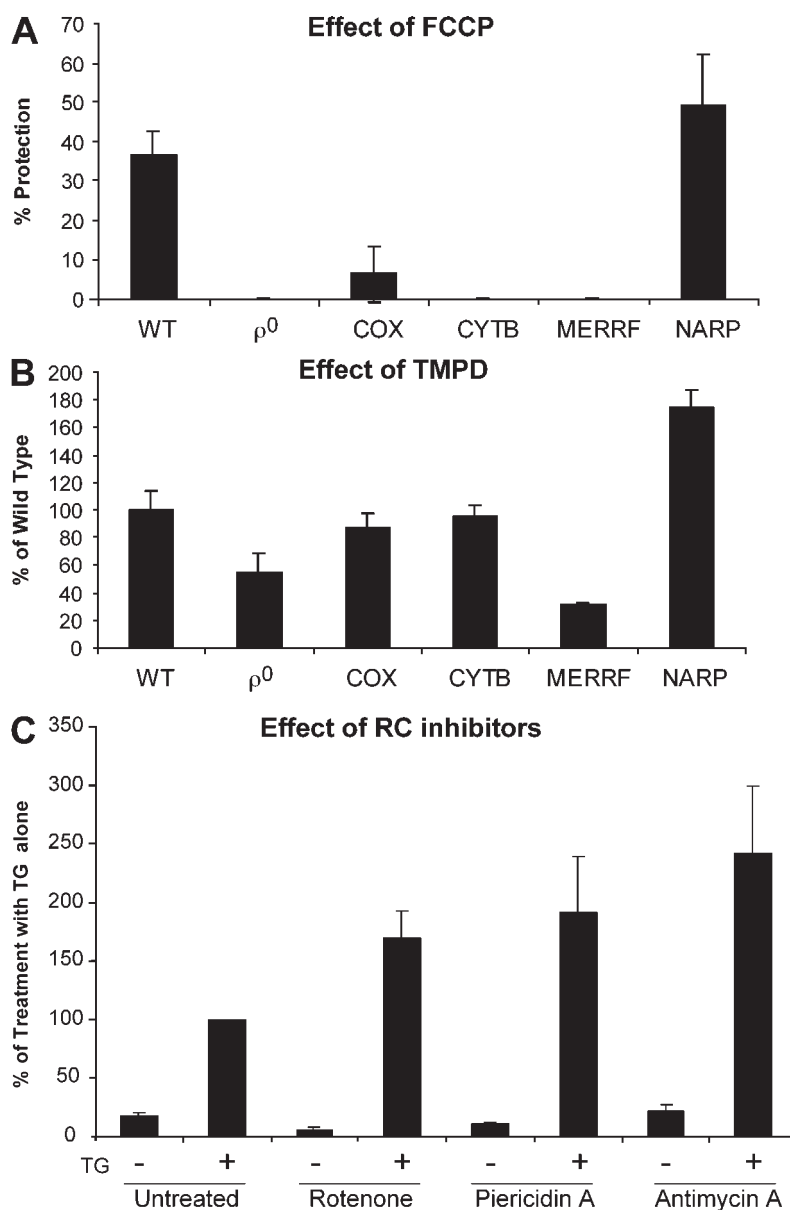
mitochondrial fractions from ρ^0 cells, which had increased Bcl-2 as compared with WT (Fig. 8 B). Interestingly, we also found that MERRF cells had a similar increase in mitochondrial Bcl-2. This suggests that, rather than the loss of mtDNA, the signal that triggers Bcl-2 up-regulation is the absence of the RC itself because MERRF cells have normal mtDNA content but are unable to synthesize RC complexes. We also found that COX cells had decreased Bcl-X_L, NARP cells had decreased Bcl-2, and CYTB cells had a decrease in both antiapoptotic proteins. Thus, cells with a defective RC and impaired electron flux have dysregulated mitochondrial levels of antiapoptotic proteins. These findings suggest that the structure and function of the electron transport chain affects the complement of antiapoptotic proteins at the mitochondria. However, if Bcl-2 was the only player involved, the responses to ER and mitochondrial stressors should follow similar patterns. Instead, we observe opposite trends in COX and CYTB mutants (Fig. 2). Therefore, Bcl-2 alone

cannot explain the different sensitivity in response to the various apoptotic stimuli.

Electron flux through the RC is protective against ER stress–induced apoptosis

To directly assess the contribution of electron flux to ER stress–induced apoptosis, cells were treated with FCCP in combination with TG. Uncoupling with FCCP allows the RC to transfer electrons at its maximal capacity, as shown by the increase in oxygen consumption in respiration-competent cells (Fig. 1 B), because it dissociates the demands of the ATP synthase from RC activity. In WT and NARP cells, FCCP treatment was protective, which is consistent with the hypothesis that increasing electron flux through the RC is protective against ER stress–induced apoptosis. This treatment had no effect in the remaining mutants as they do not have electron transfer capacity (Fig. 9 A).

COX and CYTB cells possess partially assembled RCs (Fig. 8 A) but have no electron flux. We reasoned that these cells are more sensitive to ER stress because the lack of electron flux forces the residual complexes into perpetually reduced states. Therefore, to reestablish the cycle of oxidation and reduction in the remaining complexes, we treated mutant cells with N,N,N′,N′-tetramethyl-P-phenylenediamine (TMPD), a redox mediator that can accept electrons from reduced RC complexes thereby restoring electron flux. The optimal dose of TMPD was determined in CYTB mutant cells by titrating the compound to the minimal concentration necessary to achieve the maximal KCN-sensitive respiration (unpublished data).

When TMPD was administered in combination with TG, the levels of caspase activation in COX and CYTB cells were normalized to those observed in WT cells (Fig. 9 B). As expected, ρ^0, MERRF, WT, and NARP cells were unaffected by TMPD because ρ^0 and MERRF cells do not have RCs, whereas WT and NARP cells transfer electrons independent of TMPD. Thus, this experiment confirmed that stimulation of electron flux is protective against ER stress–induced apoptosis.

Finally, we treated WT cells with the RC inhibitors rotenone, piericidin A, and antimycin A in combination with TG. Rotenone and piericidin A inihibit complex I, whereas antimycin A inhibits complex III. Pharmacological inhibition of the RC in WT cells mimics the loss of electron flux in the presence of RC complexes, which is biochemically analogous to the COX, CYTB, and NARP mutants. If loss of electron flux is proapoptotic, then RC inhibition should sensitize WT cells to TG. Indeed, the combined treatment of TG with either rotenone, piericidin A, or antimycin A resulted in increased apoptosis as compared with TG alone, whereas RC inhibitors alone had no effects (Fig. 9 C). This result is a further confirmation of the role of electron flux in modulating ER stress–induced apoptosis.

Discussion

In this study, we provide evidence that the mitochondrial RC regulates apoptosis in a context-dependent manner (Fig. 10). In the case of ER stress–induced apoptosis, blockage of the electron flux caused by partial damage to the RC (COX and CYTB cells) strongly sensitizes cells, whereas a complete absence of electron flux caused by lack of RC (ρ^0 and MERFF cells) strongly protects cells (Fig. 2, C and D). Instead, in the case of mitochondria-initiated apoptosis, both the partial (COX and CYTB cells) and complete (ρ^0 and MERFF cells) loss of RC protects cells from apoptosis (Fig. 2, A and B). These results in RC-deficient cells are in line with previous papers that showed protection against mitochondrial stressors in cells lacking mtDNA (Dey and Moraes, 2000; Lee et al., 2004; Park et al., 2004). Counterintuitively, NARP cells display heightened apoptotic responses to both the ER and mitochondrial stressors. In this case, the increased response to ER stress is likely to be ascribed to the enhanced ROS production (Fig. 7 E), whereas the increased response to mitochondrial stress can be ascribed to having a partial reduction in the electron flux while still being capable of limited RC-dependent energy production and
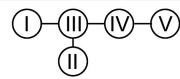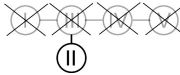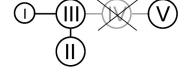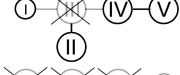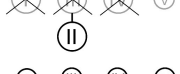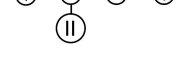
Cell Line	Respiratory Chain	STS	TG
WT	I—III—IV—V / II	+	+
ρ^0	⊗⊗⊗⊗ / II	−	−
COX	I—III—⊗—V / II	−	+++
CYTB	I—⊗—IV—V / II	−	+++
MERRF	⊗⊗⊗—v / II	−	−
NARP	I—III—IV—V / II	+++	+++

Figure 10. **Correlation between RC composition and apoptotic responses in mtDNA mutant cybrids.** The RC components of the cybrids are depicted. WT cells have a full complement of RC complexes. ρ^0 cells are missing complexes I, III, IV, and V. COX cells are missing complex IV and have reduced complex I (depicted as a smaller circle). CYTB cells are missing complex III and have reduced complex I. MERRF cells are missing complexes I, III, IV, and V, detectable by BN gel, but have some residual ATP hydrolytic complex V activity. NARP cells have all of the complexes in place, but have reduced amounts and activities. Normal response to apoptosis induction is represented by +, high response by +++, and low response by −.

oxidative phosphorylation. Therefore, our results indicate that it is not the energy production impairment per se, but rather the interplay between the stressor and a specific damage to individual components of the RC that modulate the strength of the apoptotic responses. Importantly, these patterns of response were confirmed in both cybrids derived from a different cell type (HeLa) as well as in rederived osteosarcoma cybrids (Fig. S3), suggesting that these responses are not limited to specific cell lines.

One possible explanation of how RC dysfunction is translated into global cellular effects is mitochondria-to-nucleus retrograde signaling. It has been shown that mtDNA depletion alters the transcriptional profile of cells, e.g., elevated expression of Bcl-2, Bax, Bid, and Bad (Biswas et al., 2005b), and is resistant to both STS- (Biswas et al., 2005a) and ET-mediated (Biswas et al., 2005b) cell death. Our data also show that ρ^0 cells have increased levels of Bcl-2 and are also resistant to STS and ET-mediated cell death. However, as an extension to those studies, we found that MERRF cells have increased Bcl-2, suggesting that the RC, and not the loss of mtDNA itself, is part of the signal that activates the mitochondria-to-nucleus stress response pathway. Furthermore, we find that cell lines with disrupted electron flux, such as COX, CYTB, and NARP, have dysregulated levels of Bcl-2 antiapoptotic proteins. Thus, this is an example of how the RC and electron flux cooperate to regulate the mitochondrial stress response. However, we reasoned that if Bcl-2 proteins were the only factors involved in regulating apoptosis, the differences in the patterns of response to ER and mitochondrial stress among the mutants could not be explained.

In our genetic model of RC dysfunction, mitochondrial morphological changes may also play a role in modulating the apoptotic response. Mitochondrial fusion and fission have been implicated in regulating apoptosis (Arnoult, 2007). For example, fragmentation of the mitochondrial network has been described in STS- (Karbowski et al., 2002) and ceramide-mediated (Pinton et al., 2001) apoptosis. Furthermore, upon STS treatment, Drp1, a dynamin-related protein that mediates mitochondrial outer membrane fission, translocates to mitochondria and a dominant-negative Drp1 blocks the progression of STS-induced apoptosis (Frank et al., 2001), suggesting that the mitochondrial fission machinery must be engaged for apoptosis to occur. Furthermore, down-regulation of mitochondrial fission prevents the release of cytochrome c, possibly because of the retention of soluble OPA1 (Estaquier and Arnoult, 2007), a mitochondrial fusion protein that has been shown to maintain the integrity of intracristae regions (Cipolat et al., 2006; Frezza et al., 2006) where cytochrome c is sequestered (Scorrano et al., 2002; Frezza et al., 2006).

The links between the RC, the mitochondrial remodeling machinery, and apoptosis are not yet fully understood. It has been shown that $\Delta\Psi_m$ is required to maintain normal mitochondrial morphology (Legros et al., 2002) and that ρ^0 cells have fragmented mitochondrial networks (Gilkerson et al., 2000). Consistently, we show that ρ^0, COX, CYTB, and MERRF cells, which are unable to generate RC-driven $\Delta\Psi_m$, have highly fragmented mitochondria (Fig. 3). Therefore, it could be speculated that cells with already fragmented mitochondria are protected because they are unable to normally engage the mitochondrial fission machinery upon apoptotic stimuli targeting the mitochondrial pathway. In addition, mitochondrial morphological changes may affect the way that the mitochondrial and ER networks interact. It is well known that these two organelles interact at specific contact points that are likely involved in mitochondrial–ER communication, including Ca^{2+} transfer (Csordas et al., 2006; Szabadkai et al., 2006).

How can the mitochondrion integrate environmental signals to mediate such a wide variety of responses? Our observations suggest that $\Delta\Psi_m$ and RC electron flux may be the key regulators. Accordingly, we found that stimulation of electron flux by mitochondrial uncouplers (FCCP) or electron redox mediators (TMPD) protected cells against ER stress–induced apoptosis, whereas electron flux inhibition (rotenone, piericidin A, and antimycin A) sensitized them (Fig. 9). The effect of mitochondrial uncouplers on mitochondria-initiated apoptosis in WT cells has been tested previously. A delay was observed in caspase activation by administering FCCP before the apoptotic stimulus (Stoetzer et al., 2002), but this effect was overcome if the proapoptotic stimulus was sufficiently prolonged (Lim et al., 2001), suggesting that deenergization and mitochondrial fragmentation are protective, but not completely preventive, of apoptosis.

Clearly, more work remains to be done to better understand the ramifications of this regulation at the molecular level and many potential pathways could be hypothesized for future investigation. As mentioned in the previous paragraph, $\Delta\Psi_m$ and electron flux have local effects on mitochondrial structure,

ROS production, and the components implicated in initiation of apoptosis. At the same time, they have long-ranging effects on extramitochondrial targets, such as the mitochondria-to-nucleus stress response. The latter may be performed through diffusible molecules, such as free radicals, that have known signaling functions.

Mitochondrial dysfunction and dysregulation of apoptosis have been implicated in many diseases ranging from neurodegeneration to cancer. In light of our findings, mitochondrial RC dysfunction may indeed have an important role in different disease conditions but its impact on cell survival cannot be predicted a priori. We suggest that the type of RC dysfunction will determine the predisposition toward either cell death or cell survival, depending on the environmental cues. For example, the Warburg theory proposes that mitochondrial defects may favor tumorigenesis by stimulating a glycolytic switch in metabolism and allowing survival under hypoxic conditions (Warburg, 1956). However, our data on different types of mtDNA mutations and cell death paradigms show that not all mtDNA mutations are created equal and that a simplistic model may not always hold true.

MtDNA mutations and RC dysfunction have also been associated with numerous degenerative conditions, including neurodegeneration and aging. In many of these conditions, cell death has been directly attributed to mitochondrial energy depletion. However, our data suggest that other factors, such as modulation of apoptosis, may be involved and that mtDNA mutations may not always have a negative impact on cell survival.

Importantly, the finding that manipulation of electron flux in a defective RC can modify the cell fate may lead the way toward a better understanding of the complex involvement of mitochondria in regulating cell life and death decisions. We suggest that a careful analysis of the association between the type of RC dysfunction and disease conditions should allow for a better understanding of disease pathogenesis and more effective choices in developing adequate therapeutic strategies.

Materials and methods

Reagents
All reagents used were purchased from Sigma-Aldrich unless otherwise specified.

Cell culture
Human osteosarcoma (143B) transmitochondrial cybrid cell lines were cultured in DME containing 4.5 g/liter of high glucose and supplemented with 5% FBS, 1 mM sodium pyruvate, and 50 µg/ml uridine. Cytochrome b mutant cells were provided by I.F. De Coo (Erasmus Medical Centre, Rotterdam, The Netherlands). HeLa transmitochondrial cybrid cell lines were cultured in DME (Invitrogen) containing 4.5 g/liter of high glucose and supplemented with 10% FBS, 1 mM sodium pyruvate, and 50 µg/ml uridine.

Generation of cybrid cell lines
Cybrid cell lines with a HeLa nuclear background were established by chemical enucleation. The mitochondrial donor cells containing the mtDNA genotype of interest were chemically enucleated by treatment with 0.5 µg/ml actinomycin D and then fused with HeLa ρ^0 cells as previously described (Bayona-Bafaluy et al., 2003). After fusion, cells were transferred to selection media lacking uridine to eliminate HeLa ρ^0 cells. Cybrid lines with the 143B nuclear background were also rederived using the method described for HeLa cells, except that ρ^0 143B TK cells were used as mtDNA recipients.

Oxygen consumption

The rate of oxygen consumption was measured using a Clarke-type electrode (Hansatech) as previously described (D'Aurelio et al., 2001). To measure coupled respiration, 1.5×10^6 cells were resuspended in 300 μl glucose and FBS-free DME supplemented with 1 mM sodium pyruvate. Uncoupled respiration was assessed with the addition of 1 μM FCCP and respiration was inhibited with 1.5 mM KCN.

Apoptosis assays

To induce apoptosis, cells were subjected to one of the following treatments: 1 μM STS for 6 h, 10 μM ET for 24 h, 1 μM TG for 24 h, or 1 μM TN for 24 h.

Caspase 3 activity was measured using the caspase 3 fluorogenic substrate Ac-DEVD–7-amino-4-trifluormethyl coumarin (AFC; BD Biosciences). Cells were detached, washed two times with ice-cold PBS, resuspended in 200 μl of ice-cold lysis buffer (50 mM Hepes, pH 7.4, 10 mM Chaps, 5 mM DTT, 150 mM NaCl, and 1 mM PMSF), and lysed on ice for 20 min. Lysates were centrifuged for 10 min at 16,000 g and the supernatant was retained. 10 μl of the supernatant was incubated with 100 μl of reaction buffer (50 mM Hepes, pH 7.4, 0.25% Chaps, 150 mM NaCl, 10% sucrose, 5 mM DTT, and 0.05 mg/ml Ac-DEVD-AFC) for 1 h at 37°C. Ac-DEVD-AFC fluorescence was monitored using a plate reader (HTS7000; PerkinElmer) with excitation at 400 nm and emission at 485 nm, and readings were expressed as fluorescence per microgram of protein.

To count apoptotic nuclei, cells were plated on glass coverslips, treated with the various apoptosis inducing agents, fixed with 4% paraformaldehyde for 15 min, and stained with 1 μg/ml HOECHST 33342 (Invitrogen) diluted in PBS for 5 min. Nuclear morphology was assessed by fluorescence microscopy to determine the proportion of cells with apoptotic (i.e., fragmented and/or condensed) nuclei.

To detect cells undergoing apoptosis, cells were stained using the Annexin-V-FLUOS staining kit (Roche) as per the manufacturer's instructions and evaluated by fluorescence microscopy. The proportion of apoptotic cells was determined by counting cells that stained positive for annexin V (excitation 488 nm; emission 518 nm) and negative for propidium iodide (excitation 488 nm; emission 617 nm), whereas necrotic cells stained positive for both annexin V and propidium iodide.

Cell viability assays

A WST-1 cell proliferation reagent (Roche) was used to measure cell viability after treatment with proapoptotic compounds. Cells were plated onto 96-well plates in triplicates, allowed to attach for 8 h, and then subjected to treatment with 1 μM STS for 3.5 h, 10 μM ET for 24 h, or 1 μM TG for 24 h. 20 μl WST-1 was added to each well and incubated for 2 h at 37°C. Changes in WST-1 absorbance were measured at 450 nm in a plate reader.

Free radical production

Free radical production was measured using 2′,7′-dichlorofluorescin diacetate (H$_2$DCFDA; Invitrogen). Cells were grown in 48-well plates, loaded with 20 μM H$_2$DCFDA for 2 h at 37°C, and then lysed with 0.2% Triton X-100. H$_2$DCFDA fluorescence was measured in a HTS7000 plate reader (excitation 485 nm; emission 535 nm). Free radical production was expressed as the fluorescence normalized by the protein content of the sample.

Confocal microscopy and image analysis

For confocal microscopy, cells were grown in 4-well chambers, stained with 100 nM MitoTracker Red CMXRos (Invitrogen) for 30 min at 37°C, and washed three times with PBS. Cells were imaged in PBS at room temperature using a laser-scanning confocal microscope (LSM 510; Carl Zeiss, Inc.) with a 63× Plan Apochromat oil immersion lens with aperture 1.4 using a photomultiplier (Carl Zeiss, Inc.). The excitation wavelength for MitoTracker Red CMXRos was 488 nm. A series of z-sections were taken spanning the thickness of the cell with intervals between sections set at 0.5 μm. Z-stack images were projected onto a single plane using the LSM Image Browser software (Carl Zeiss, Inc.). Digital magnification was 2× (total magnification was 126×). Image analysis and mitochondrial length measurements were performed on the projected images using Metamorph software (MDS Analytical Technologies).

Measurements of cellular ATP content

Cellular ATP content was measured using the Enliten rLuciferase/Luciferin Reagent (Promega). Cells were seeded on 96-well plates and grown overnight. Luminescence was measured according to the manufacturer's protocol in a luminometer (MGM Instruments). A standard curve was constructed with known ATP concentrations ranging from 100 pico M to 1 mM.

Cytosolic Ca^{2+} measurements in intact cells

Cytosolic Ca^{2+} levels were monitored using the fluorescent ratiometric dye Fura 2AM (Invitrogen). Ca^{2+}-free incubation buffer was composed of 145 mM NaCl, 2.8 mM KCl, 2 mM MgCl$_2$, 10 mM glucose, and 10 mM Hepes, pH 7.4. Cells were trypsinized and resuspended in incubation buffer at a concentration of 10^6 cells/ml and loaded with 5 μM Fura 2AM for 30 min at room temperature. Cells were then washed with incubation buffer and resuspended at a concentration of 3×10^5 cells/ml in Ca^{2+} reaction buffer (2 mM CaCl$_2$, 145 mM NaCl, 2.8 mM KCl, 2 mM MgCl$_2$, 10 mM glucose, and 10 mM Hepes, pH 7.4). Fura 2AM fluorescence was measured in a fluorimeter cuvette with constant stirring, and recorded at 340/380 nm excitation and 512 nm emission with a fluorescence spectrophotometer (F-4500; Hitachi). Ca^{2+} was released from the ER using 1 μM TG and from mitochondria using 2.5 μM FCCP. The ratio of Fura 2AM fluorescence was plotted against time.

Ca^{2+} uptake in isolated mitochondria

Ca^{2+} uptake was measured in enriched mitochondrial fractions using the dye Calcium Green-5N (Invitrogen). Enriched mitochondrial fractions were prepared by harvesting cells in MS-EGTA buffer (225 mM mannitol, 75 mM sucrose, 5 mM Hepes, and 1 mM EGTA, pH 7.4, with KOH), homogenization with a Dounce homogenizer, and differential centrifugation. Homogenate was first centrifuged at 2,000 g for 5 min at 4°C. The supernatant was then centrifuged at 14,000 g for 10 min at 4°C. The resulting mitochondrial pellet was kept on ice. Mitochondria were incubated in KCl buffer (125 mM KCl, 20 mM Hepes, 2 mM MgCl$_2$, 2 mM potassium phosphate, and 40 μM EGTA, pH 7.2, with KOH) containing 200 nM Calcium Green-5N and either 1 mM pyruvate and 7 mM malate or 4 mM ATP. Mitochondria were challenged with sequential CaCl$_2$ additions and calcium uptake was monitored in a fluorescence spectrophotometer.

ΔΨ$_m$

The ability to generate ΔΨ$_m$ was assessed in enriched mitochondrial fractions using the dye safranin-O as previously described (Akerman and Wikstrom, 1976; Kowaltowski et al., 2002) with modifications. Enriched mitochondrial fractions were prepared by harvesting cells in MS-EGTA buffer and homogenizing using a dounce homogenizer. Cell homogenate was first centrifuged at 600 g for 5 min to pellet nuclei and unbroken cells. The supernatant was then removed and centrifuged at 10,000 g for 10 min to pellet mitochondria. The mitochondrial pellet was resuspended in MS-EGTA buffer. Mitochondria were incubated with safranin-O at a ratio of 20:1 (dye/mitochondrial protein; Zanotti and Azzone, 1980) in 1 ml KCl buffer. Safranin-O fluorescence was monitored in a fluorimeter cuvette with constant stirring and recorded at 485 nm excitation and 586 nm emission. 2 mM ATP was added to the reaction to measure the ATP hydrolysis–supported ΔΨ$_m$. Where indicated, mitochondria were deenergized by inhibiting the ADP–ATP exchange with 1.3 μM carboxyatractylate, a specific inhibitor of the adenine nucleotide transporter. To assess the RC-dependent generation of ΔΨ$_m$, the incubation medium was supplemented with 5 mM succinate. Where indicated, mitochondria were deenergized by blocking the electron transport at RC complex III with 1 μM of its specific inhibitor antimycin A.

BN gels

BN PAGE followed by immunodetection was used to identify individual RC complexes. Mitochondrial membranes were prepared by permeabilizing 2.5×10^6 cells with 0.2% wt/vol digitonin (Sigma-Aldrich) for 10 min on ice as previously described (Nijtmans et al., 2002). 10 μl of sample were loaded on a 5–13% gradient polyacrylamide gel and electrophoresis was performed as previously described (Nijtmans et al., 2002). Transfer of proteins onto polyvinylidine fluoride (PVDF) membrane (Bio-Rad Laboratories) was performed overnight at 30 V at 4°C. For immunodetection of the protein complexes, monoclonal antibodies (Invitrogen) against the following RC complexes were used: the 39-kD subunit of complex I, the 70-kD subunit of complex II, the core 2 subunit of complex III, subunit I of complex IV, and the β subunit of complex V.

Western blotting

For Western blots of total cellular protein, cells were lysed on ice with 25 mM Tris-HCl, pH 7.6, 150 mM NaCl, 1% NP-40, and 1% sodium deoxycholate, and 0.1% SDS and protein concentrations were measured (Bio-Rad Laboratories). Equal amounts of protein were separated by SDS-PAGE

and transferred to PVDF membranes. Membranes were then blocked with 5% nonfat milk in 0.1% TBS–tween 20 and probed with specific antibodies (BD Biosciences) against Grp78 (1:250), Tim23 (1:5,000), caspase 3 (1:1,000), and caspase 9 (1:1,000).

For Western blots of enriched mitochondrial fractions prepared by subcellular fractionation and differential centrifugation, 10^7 cells were trypsinized and washed in ice-cold NKM buffer (130 mM NaCl, 5 mM KCl, and 7.5 mM $MgCl_2$). Cells were then resuspended in RSB buffer (10 mM Tris-HCl, pH 7.6, 10 mM KCl, and 0.15 mM $MgCl_2$) and swelled for 4 min on ice before homogenization with a glass Dounce homogenizer. Sucrose was then added to a final concentration of 500 mM. The total cell homogenate was then centrifuged at 600 g for 10 min at 4°C, and the supernatant was centrifuged at 15,000 g for 15 min at 4°C to pellet the mitochondria. Equal amounts of mitochondrial protein were loaded and resolved by electrophoresis in a 10% SDS–polyacrylamide gel, and then transferred to PVDF membranes. Membranes were blocked with 5% nonfat milk in TBS–tween 20 (0.1%) and probed with specific antibodies against Bcl-2 (1:1,000; Santa Cruz Biotechnology, Inc.), BclX$_L$ (1:1,000; Santa Cruz Biotechnology, Inc.), Tim23 (1:5,000; BD Biosciences), Hsp60 (1:2,500; Assay Designs), and VDAC (1:5,000; EMD). Membranes were then incubated with HRP-conjugated secondary antibodies and developed with a chemiluminescent reagent (Thermo Fisher Scientific).

Online supplemental material
Fig. S1 shows percentage of apoptotic nuclei in cells treated with STS and cells undergoing apoptosis upon treatment with TG. Fig. S2 shows Western blots of caspase 9 and 3 and cell survival assays. Fig. S3 shows caspase 3 activity in response to TG and caspase 3 activity in response to TG in HeLa WT and HeLa ρ^0 cells. Online supplemental material is available at http://www.jcb.org/cgi/content/full/jcb.200704059/DC1.

References

Acin-Perez, R., M.P. Bayona-Bafaluy, P. Fernandez-Silva, R. Moreno-Loshuertos, A. Perez-Martos, C. Bruno, C.T. Moraes, and J.A. Enriquez. 2004. Respiratory complex III is required to maintain complex I in mammalian mitochondria. *Mol. Cell.* 13:805–815.

Akerman, K.E., and M.K. Wikstrom. 1976. Safranine as a probe of the mitochondrial membrane potential. *FEBS Lett.* 68:191–197.

Anderson, S., A.T. Bankier, B.G. Barrell, M.H. de Bruijn, A.R. Coulson, J. Drouin, I.C. Eperon, D.P. Nierlich, B.A. Roe, F. Sanger, et al. 1981. Sequence and organization of the human mitochondrial genome. *Nature.* 290:457–465.

Arnoult, D. 2007. Mitochondrial fragmentation in apoptosis. *Trends Cell Biol.* 17:6–12.

Bayona-Bafaluy, M.P., G. Manfredi, and C.T. Moraes. 2003. A chemical enucleation method for the transfer of mitochondrial DNA to rho(o) cells. *Nucleic Acids Res.* 31:e98.

Biswas, G., H.K. Anandatheerthavarada, and N.G. Avadhani. 2005a. Mechanism of mitochondrial stress-induced resistance to apoptosis in mitochondrial DNA-depleted C2C12 myocytes. *Cell Death Differ.* 12:266–278.

Biswas, G., M. Guha, and N.G. Avadhani. 2005b. Mitochondria-to-nucleus stress signaling in mammalian cells: nature of nuclear gene targets, transcription regulation, and induced resistance to apoptosis. *Gene.* 354:132–139.

Bruno, C., A. Martinuzzi, Y. Tang, A.L. Andreu, F. Pallotti, E. Bonilla, S. Shanske, J. Fu, C.M. Sue, C. Angelini, et al. 1999. A stop-codon mutation in the human mtDNA cytochrome c oxidase I gene disrupts the functional structure of complex IV. *Am. J. Hum. Genet.* 65:611–620.

Chatterjee, A., E. Mambo, and D. Sidransky. 2006. Mitochondrial DNA mutations in human cancer. *Oncogene.* 25:4663–4674.

Cipolat, S., T. Rudka, D. Hartmann, V. Costa, L. Serneels, K. Craessaerts, K. Metzger, C. Frezza, W. Annaert, L. D'Adamio, et al. 2006. Mitochondrial rhomboid PARL regulates cytochrome c release during apoptosis via OPA1-dependent cristae remodeling. *Cell.* 126:163–175.

Cortes-Hernandez, P., M.E. Vazquez-Memije, and J.J. Garcia. 2007. ATP6 homoplasmic mutations inhibit and destabilize the human F1F0-ATP synthase without preventing enzyme assembly and oligomerization. *J. Biol. Chem.* 282:1051–1058.

Csordas, G., C. Renken, P. Varnai, L. Walter, D. Weaver, K.F. Buttle, T. Balla, C.A. Mannella, and G. Hajnoczky. 2006. Structural and functional features and significance of the physical linkage between ER and mitochondria. *J. Cell Biol.* 174:915–921.

D'Aurelio, M., F. Pallotti, A. Barrientos, C.D. Gajewski, J.Q. Kwong, C. Bruno, M.F. Beal, and G. Manfredi. 2001. In vivo regulation of oxidative phosphorylation in cells harboring a stop-codon mutation in mitochondrial DNA-encoded cytochrome c oxidase subunit I. *J. Biol. Chem.* 276:46925–46932.

D'Aurelio, M., C.D. Gajewski, G. Lenaz, and G. Manfredi. 2006. Respiratory chain supercomplexes set the threshold for respiration defects in human mtDNA mutant cybrids. *Hum. Mol. Genet.* 15:2157–2169.

Danial, N.N., and S.J. Korsmeyer. 2004. Cell death: critical control points. *Cell.* 116:205–219.

De Coo, I.F., W.O. Renier, W. Ruitenbeek, H.J. Ter Laak, M. Bakker, H. Schagger, B.A. Van Oost, and H.J. Smeets. 1999. A 4-base pair deletion in the mitochondrial cytochrome b gene associated with parkinsonism/MELAS overlap syndrome. *Ann. Neurol.* 45:130–133.

Dey, R., and C.T. Moraes. 2000. Lack of oxidative phosphorylation and low mitochondrial membrane potential decrease susceptibility to apoptosis and do not modulate the protective effect of Bcl-x(L) in osteosarcoma cells. *J. Biol. Chem.* 275:7087–7094.

DiMauro, S., and E.A. Schon. 2003. Mitochondrial respiratory-chain diseases. *N. Engl. J. Med.* 348:2656–2668.

Estaquier, J., and D. Arnoult. 2007. Inhibiting Drp1-mediated mitochondrial fission selectively prevents the release of cytochrome c during apoptosis. *Cell Death Differ.* 14:1086–1094.

Frank, S., B. Gaume, E.S. Bergmann-Leitner, W.W. Leitner, E.G. Robert, F. Catez, C.L. Smith, and R.J. Youle. 2001. The role of dynamin-related protein 1, a mediator of mitochondrial fission, in apoptosis. *Dev. Cell.* 1:515–525.

Frezza, C., S. Cipolat, O. Martins de Brito, M. Micaroni, G.V. Beznoussenko, T. Rudka, D. Bartoli, R.S. Polishuck, N.N. Danial, B. De Strooper, and L. Scorrano. 2006. OPA1 controls apoptotic cristae remodeling independently from mitochondrial fusion. *Cell.* 126:177–189.

Geromel, V., N. Kadhom, I. Cebalos-Picot, O. Ouari, A. Polidori, A. Munnich, A. Rotig, and P. Rustin. 2001. Superoxide-induced massive apoptosis in cultured skin fibroblasts harboring the neurogenic ataxia retinitis pigmentosa (NARP) mutation in the ATPase-6 gene of the mitochondrial DNA. *Hum. Mol. Genet.* 10:1221–1228.

Gilkerson, R.W., D.H. Margineantu, R.A. Capaldi, and J.M. Selker. 2000. Mitochondrial DNA depletion causes morphological changes in the mitochondrial reticulum of cultured human cells. *FEBS Lett.* 474:1–4.

Holt, I.J., A.E. Harding, R.K. Petty, and J.A. Morgan-Hughes. 1990. A new mitochondrial disease associated with mitochondrial DNA heteroplasmy. *Am. J. Hum. Genet.* 46:428–433.

Izyumov, D.S., A.V. Avetisyan, O.Y. Pletjushkina, D.V. Sakharov, K.W. Wirtz, B.V. Chernyak, and V.P. Skulachev. 2004. "Wages of fear": transient threefold decrease in intracellular ATP level imposes apoptosis. *Biochim. Biophys. Acta.* 1658:141–147.

Karbowski, M., Y.J. Lee, B. Gaume, S.Y. Jeong, S. Frank, A. Nechushtan, A. Santel, M. Fuller, C.L. Smith, and R.J. Youle. 2002. Spatial and temporal association of Bax with mitochondrial fission sites, Drp1, and Mfn2 during apoptosis. *J. Cell Biol.* 159:931–938.

King, M.P., and G. Attardi. 1989. Human cells lacking mtDNA: repopulation with exogenous mitochondria by complementation. *Science.* 246:500–503.

Kowaltowski, A.J., R.G. Cosso, C.B. Campos, and G. Fiskum. 2002. Effect of Bcl-2 overexpression on mitochondrial structure and function. *J. Biol. Chem.* 277:42802–42807.

Kujoth, G.C., C. Leeuwenburgh, and T.A. Prolla. 2006. Mitochondrial DNA mutations and apoptosis in mammalian aging. *Cancer Res.* 66:7386–7389.

Kwong, J.Q., M.F. Beal, and G. Manfredi. 2006. The role of mitochondria in inherited neurodegenerative diseases. *J. Neurochem.* 97:1659–1675.

Lee, M.S., J.Y. Kim, and S.Y. Park. 2004. Resistance of rho(0) cells against apoptosis. *Ann. NY Acad. Sci.* 1011:146–153.

Legros, F., A. Lombes, P. Frachon, and M. Rojo. 2002. Mitochondrial fusion in human cells is efficient, requires the inner membrane potential, and is mediated by mitofusins. *Mol. Biol. Cell.* 13:4343–4354.

Li, J., B. Lee, and A.S. Lee. 2006. Endoplasmic reticulum stress-induced apoptosis: multiple pathways and activation of p53-up-regulated modulator of apoptosis (PUMA) and NOXA by p53. *J. Biol. Chem.* 281:7260–7270.

Lim, M.L., T. Minamikawa, and P. Nagley. 2001. The protonophore CCCP induces mitochondrial permeability transition without cytochrome c release in human osteosarcoma cells. *FEBS Lett.* 503:69–74.

Mattiazzi, M., C. Vijayvergiya, C.D. Gajewski, D.C. DeVivo, G. Lenaz, M. Wiedmann, and G. Manfredi. 2004. The mtDNA T8993G (NARP) mutation results in an impairment of oxidative phosphorylation that can be improved by antioxidants. *Hum. Mol. Genet.* 13:869–879.

Nijtmans, L.G., N.S. Henderson, and I.J. Holt. 2002. Blue Native electrophoresis to study mitochondrial and other protein complexes. *Methods*. 26:327–334.

Park, S.Y., I. Chang, J.Y. Kim, S.W. Kang, S.H. Park, K. Singh, and M.S. Lee. 2004. Resistance of mitochondrial DNA-depleted cells against cell death: role of mitochondrial superoxide dismutase. *J. Biol. Chem.* 279:7512–7520.

Pinton, P., D. Ferrari, E. Rapizzi, F. Di Virgilio, T. Pozzan, and R. Rizzuto. 2001. The Ca^{2+} concentration of the endoplasmic reticulum is a key determinant of ceramide-induced apoptosis: significance for the molecular mechanism of Bcl-2 action. *EMBO J.* 20:2690–2701.

Polyak, K., Y. Li, H. Zhu, C. Lengauer, J.K. Willson, S.D. Markowitz, M.A. Trush, K.W. Kinzler, and B. Vogelstein. 1998. Somatic mutations of the mitochondrial genome in human colorectal tumours. *Nat. Genet.* 20:291–293.

Scorrano, L., M. Ashiya, K. Buttle, S. Weiler, S.A. Oakes, C.A. Mannella, and S.J. Korsmeyer. 2002. A distinct pathway remodels mitochondrial cristae and mobilizes cytochrome *c* during apoptosis. *Dev. Cell*. 2:55–67.

Spierings, D., G. McStay, M. Saleh, C. Bender, J. Chipuk, U. Maurer, and D.R. Green. 2005. Connected to death: the (unexpurgated) mitochondrial pathway of apoptosis. *Science*. 310:66–67.

Stoetzer, O.J., A. Pogrebniak, R. Pelka-Fleischer, M. Hasmann, W. Hiddemann, and V. Nuessler. 2002. Modulation of apoptosis by mitochondrial uncouplers: apoptosis-delaying features despite intrinsic cytotoxicity. *Biochem. Pharmacol.* 63:471–483.

Szabadkai, G., K. Bianchi, P. Varnai, D. De Stefani, M.R. Wieckowski, D. Cavagna, A.I. Nagy, T. Balla, and R. Rizzuto. 2006. Chaperone-mediated coupling of endoplasmic reticulum and mitochondrial Ca^{2+} channels. *J. Cell Biol.* 175:901–911.

Wallace, D.C., X.X. Zheng, M.T. Lott, J.M. Shoffner, J.A. Hodge, R.I. Kelley, C.M. Epstein, and L.C. Hopkins. 1988. Familial mitochondrial encephalomyopathy (MERRF): genetic, pathophysiological, and biochemical characterization of a mitochondrial DNA disease. *Cell*. 55:601–610.

Warburg, O. 1956. On respiratory impairment in cancer cells. *Science*. 124:269–270.

Xu, C., B. Bailly-Maitre, and J.C. Reed. 2005. Endoplasmic reticulum stress: cell life and death decisions. *J. Clin. Invest.* 115:2656–2664.

Zanotti, A., and G.F. Azzone. 1980. Safranine as membrane potential probe in rat liver mitochondria. *Arch. Biochem. Biophys.* 201:255–265.